





# Linear Stark effect in $\text{Y}_3\text{Al}_5\text{O}_{12} : \text{Tm}^{3+}$ crystal and its application in the addressable quantum memory protocol

M. M. Minnegaliev <sup>1</sup>, K. I. Gerasimov <sup>1</sup>, R. V. Urmancheev <sup>1</sup>, A. M. Zheltikov,<sup>1,2,3,4</sup> and S. A. Moiseev <sup>1,\*</sup>

<sup>1</sup>*Kazan Quantum Center, Kazan National Research Technical University, n.a. A.N. Tupolev-KAI, 10 K. Marx St., 420111 Kazan, Russia*

<sup>2</sup>*Physics Department, M.V. Lomonosov Moscow State University, Moscow 119991, Russia*

<sup>3</sup>*Department of Physics and Astronomy, Texas A&M University, College Station, Texas 77843, USA*

<sup>4</sup>*Russian Quantum Center, Skolkovo, Moscow Region 143025, Russia*



(Received 26 February 2021; accepted 20 April 2021; published 18 May 2021)

We report an observation of the linear Stark effect in a  $\text{Tm}^{3+} : \text{Y}_3\text{Al}_5\text{O}_{12}$  crystal with the distribution of the Stark coefficient over the ion ensemble. We associate this effect with local lattice distortions near the positions of  $\text{Tm}^{3+}$  ions. Using this effect, the addressable storage of a series of weak light pulses in a cavity-assisted scheme of the revival of silenced echo quantum memory protocol is implemented. In this memory scheme, we also demonstrate storage of a light pulse on the few photon level. The application of an optical resonator makes it possible to increase the memory efficiency in this crystal and to reduce the minimal number of photons in the input signal pulse to 5.6 for the signal-to-noise ratio of 1 in the retrieved echo pulse. The results are in good agreement with the theoretical analysis. The possible ways of the further improvement of the implemented memory scheme are also discussed.

DOI: [10.1103/PhysRevB.103.174110](https://doi.org/10.1103/PhysRevB.103.174110)

## I. INTRODUCTION

Optical quantum memory (QM) [1–4] plays an important role in the creation of a quantum network [5] and long-distance quantum communication using a quantum repeater [6]. Solid-state QMs [7] based on various spectral modifications of the reversible photon echo [8] have proven to be suitable for the storage of multipulse light fields as they were used to store more than 1000 light pulses [9]. Crystals doped with rare-earth ions (REI) [7] possess a unique combination of a long coherence time and inhomogeneous broadening of optical transitions [10,11], which is interesting for the implementation of broadband QM and increasing its storage capacity. Moreover, it seems possible to implement an extremely long coherence time on the electron-nuclear spin states in such crystals [12–14] that promises the creation of a long-lived multimode optical and microwave QM and repeater required for quantum computing and long-distance quantum communication.

The thulium ion is one of the interesting REIs for QM implementation, which has an  $^3\text{H}_6(0) \rightarrow ^3\text{H}_4(0)$  optical transition with a wavelength  $\lambda \sim 790\text{--}800$  nm in the third transparency window of commercial optical fiber. This transition has a wide inhomogeneous broadening in garnet crystals at cryogenic temperatures [20 GHz in  $\text{Y}_3\text{Al}_5\text{O}_{12}$  (YAG) and 56 GHz in  $\text{Y}_3\text{Ga}_5\text{O}_{12}$  (YGG)], which can be used for implementation of broadband QM [9]. The coherence times of this optical transition of  $\sim 75$   $\mu\text{s}$  in YAG [15] and  $\sim 220$   $\mu\text{s}$  in YGG [16] in zero magnetic field are sufficient to investigate and develop QM protocols. The optical coherence time can be even increased to 350 and 490  $\mu\text{s}$ , respectively, by applying

low magnetic fields [17,18]. This set of parameters allows the implementation of various quantum memory protocols in the  $\text{Tm} : \text{YAG}$  crystal [19,20]. One of them is the revival of silenced echo (ROSE) protocol [21–23].

The ROSE protocol has several potential advantages in the implementation of QM in optical and microwave spectral domains [21,23,24]. First, this protocol makes it possible to use the natural inhomogeneous broadening of the atomic transition; it does not require the additional spectral preparation of initial atomic states as, e.g., in the atomic frequency comb (AFC) protocol or in CRIB/GEM protocols [2–4,7,25]. Second, the storage time of QM in the ROSE protocol is mainly affected by the coherence time (including instantaneous spectral diffusion effects [17,26]) of the atoms themselves. For comparison, in two-level versions of GEM and AFC protocols, the storage time is determined by the spectral width of a specially prepared single narrow resonant line, or of the atomic frequency combs, which cannot be narrower than the atomic spectral linewidth. As a consequence, longer storage times and on-demand retrieval are easier to achieve using the ROSE protocol. It is worth noting that the ROSE protocol, like AFC and GEM, can be also performed in the spin-wave scheme, which significantly increases the storage time of these QMs. Third, the retrieval of the stored light can be implemented by using just two rephasing control  $\pi$  pulses. As a consequence, longer storage times and on-demand retrieval are easier to achieve using the ROSE protocol.

A perfect implementation of the ROSE protocol requires the elimination of excessive excitation of atoms on the optically excited levels to suppress the appearance of optical quantum noise in the echo signal, which is the most critical issue of the ROSE protocol. One of the important requirements is the suppression of the primary echo signal emitted after the first control  $\pi$  pulse, as well as preparing

\*s.a.moiseev@kazanqc.org

$\pi$  pulses as close to ideal as possible to suppress spontaneous emission of noise photons after the two control  $\pi$  pulses. Spatial phase mismatching can be used to suppress the primary echo signal [21]. For example, the transverse (orthogonal) geometry of the propagation of control and signal light beams ensures that the primary echo is suppressed and the ROSE echo is emitted [27]. In this geometry, rephased amplified spontaneous emission [28] is also suppressed in the signal field propagation direction due to the phase mismatching. Another way to suppress the primary echo is to use the Stark (or Zeeman) effect for controllable spectral dephasing/rephasing of the atomic coherence. It is known as hybrid photon-echo rephasing (HYPER) [29] and Stark echo modulation [30] QM protocols in the optical and microwave domains, respectively. Using dc Stark gradient fields are also well elaborated for the implementation of the controlled reversible inhomogeneous broadening (CRIB) protocol [8,25] in the gradient echo memory QM scheme [31,32]. Combining the dc Stark shift and the ac Stark shift (light shift) makes an even more versatile tool for the coherence control in QM [33–37].

External electric or magnetic field gradient pulses can also be used to build an addressing protocol as it was demonstrated for optical QM in the Rb-gas system [38] and microwave AFC-type memory scheme in liquid (tetracyanoethylene anion radicals in toluene) [39]. Efficient addressing of each qubit is an essential tool for multiqubit QM, in particular, in the elaboration of quantum random access memories [40,41] and efficient multiplexing operation in a quantum repeater [6,42]. However, addressing in solid-state QM remains poorly developed experimentally and requires further improvement along with the creation of more sufficient QM schemes.

An initial experiment with the ROSE protocol demonstrated the optical storage of few-photon fields in the  $\text{Tm}^{3+} : \text{Y}_3\text{Al}_5\text{O}_{12}$  crystal in the free space configuration [22]. In this experiment, the input signal pulse contained 14 photons and the retrieved echo pulse contained about 1.4 photon with the signal/noise ratio of 1, which indicates the need for further significant improvement of this protocol for its use in QM of single-photon fields. A possible way to improve the ROSE protocol implementation is to place the atomic medium inside an impedance-matched optical cavity [43,44] or multi-resonator system [41,45] with spectrally matched parameters. This makes it possible to reduce the working number of atoms and potentially suppress the optical noise of atomic spontaneous emission which is proportional to the total number of atoms. The described advantages were partially implemented in recent works [20,35,46–48] devoted to the development of the cavity-assisted impedance-matched AFC protocol.

In this work, we focus on the development of the addressable QM in crystals based on the ROSE protocol in the impedance-matched scheme. Initially, we observed the linear dc Stark effect in  $\text{Tm}^{3+} : \text{Y}_3\text{Al}_5\text{O}_{12}$  crystal placed in a uniform external electric field, despite the symmetry properties of the original crystal cell. We assume that each  $\text{Tm}^{3+}$  ion gets its own linear Stark shift, which is determined by the features of the deformation of its local environment. Then, taking advantage of this phenomenon, we implemented a cavity-assisted ROSE protocol in the  $\text{Tm}^{3+} : \text{Y}_3\text{Al}_5\text{O}_{12}$  crystal with efficient addressing in the storage and retrieval of individual light pulses in the multipulse memory. In addition, in this memory

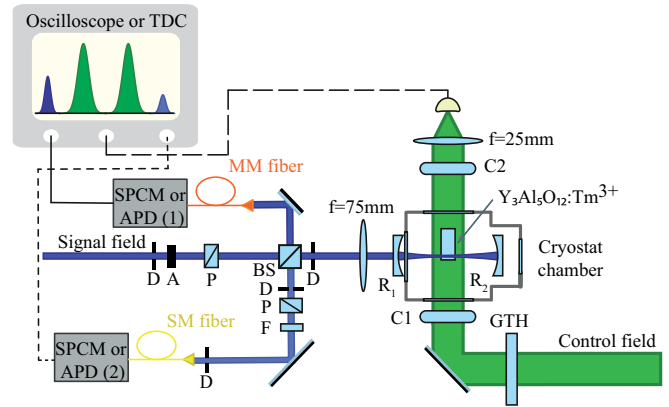


FIG. 1. Simplified sketch of the experimental setup:  $R_1$  and  $R_2$  denote front and back mirror of the concentric resonator; P, Glan-Taylor polarizer; D, diaphragm; A, neutral density filter; BS, 50:50 beam splitter; F, fluorescence bandpass filter; MM, multimode fiber; SM, single mode fiber; SPCM, single photon counting module; APD, avalanche photodetector; TDC, time to digital converter; C, cylindrical lens; f, spherical lens; GTH, Gauss to top hat beam shaping lens.

scheme, we improved the ROSE protocol for the storage of few photon light fields. Here, it was possible to store a signal light pulse containing 5.6 photons with a signal-to-noise ratio of 1 in the retrieved echo pulse, which is about 2.5 times less than in the previous demonstration of this protocol in the free space [22]. Finally, we discuss the possible ways to further improve the implemented cavity-assisted multimode memory scheme.

## II. EXPERIMENTAL SETUP

A simplified scheme of the experimental setup is shown in Fig. 1. The  $\text{Tm}^{3+} : \text{Y}_3\text{Al}_5\text{O}_{12}$  ( $c = 0.1$  at. %) crystal with dimensions of  $2 \times 3 \times 8$  mm and edges parallel to the [110], [001], and  $[\bar{1}10]$  crystallographic axes, respectively, played a role of the optical memory cell. The faces parallel to the (001) and  $(\bar{1}10)$  crystallographic planes were polished with the surface roughness of  $\sim \lambda/8$  and AR coated. The faces parallel to the (110) plane were polished with the surface roughness of  $\sim \lambda/2$ . The crystal was placed in a closed-cycle cryostat (Montana Instruments Corp.), where it was cooled down to  $3.7 \pm 0.05$  K.

We used the  ${}^3\text{H}_6(0) \rightarrow {}^3\text{H}_4(0)$  optical transition of  $\text{Tm}^{3+}$  having the inhomogeneous linewidth of  $\sim 20$  GHz and coherence (or phase-memory) time of  $T_M = 70 \pm 2$   $\mu\text{s}$  with  $x = 1.6 \pm 0.1$ . Here, we follow the approach of Mims [49] describing the nonexponential dependence of the two pulse spin echo intensity in the presence of spectral diffusion as  $I = I_0 \exp\{-2(2\tau/T_M)^x\}$  versus time delay  $\tau$  between the first and second exciting pulses. The signal and control laser fields propagated along the [001] ( $l = 3$  mm edge of the crystal) and  $[\bar{1}10]$  (8 mm edge of the crystal) axes, respectively, both polarized along the [110] crystal axis. Under these conditions, we measured the absorption coefficient in the center of the inhomogeneous broadening of the  ${}^3\text{H}_6(0) \rightarrow {}^3\text{H}_4(0)$  optical transition ( $\nu = 377.867$  THz)  $\alpha = 1.75$   $\text{cm}^{-1}$  for the signal field polarized along the [110] axis.

The concentric optical cavity consisted of two spherical dielectric mirrors having the reflection coefficients of  $R_1 = 70\%$  for the front mirror and  $R_2 \approx 99.9\%$  for the back one. The total length of the resonator was  $L = 90$  mm, which corresponded to the free spectral range of 1.65 GHz. In this case, the impedance-matching condition was achieved for absorption of  $\alpha_0 l = 0.15$ , where  $l$  is the length of the crystal and  $\alpha_0$  is an absorption coefficient at the chosen frequency. The best matching condition was achieved at 377.879 THz frequency at the edge of the absorption line of thulium ions. The finesse of the resonator measured outside the absorption line was  $F = 14.5 \pm 0.5$ , that was in reasonable agreement with the ideal  $F_0 = 17.5$  considering losses inside the cavity. More information and graphs concerning the impedance-matching condition can be found in the Supplemental Material [50].

Our crystal did not have the best orientation for the implementation of the photon echo QM in the orthogonal geometry. Tm ions in the  $Y_3Al_5O_{12}$  crystal have six orientationally inequivalent sites [51]. It is assumed that the control field interacts with the same subgroups of ions as the signal field. This is possible for such crystal orientation, with the polarization of both beams along the [110] axis of the crystal. However, in this case, there are two types of ion sites for both light fields with different Rabi frequencies that reduce the effectiveness of the rephasing pulses if ordinary  $\pi$  pulses are used. To overcome this issue in all ROSE protocol implementations, we used complex hyperbolic secant (CHS) pulses [52,53] implemented under adiabatic rapid passage conditions [54,55]. The electric field of these pulses ( $m = 1, 2$ ) is defined by

$$\begin{aligned} \mathbf{E}_m(t, \mathbf{r}) = & \frac{1}{2} \mathbf{e}_c \varepsilon(t - t_m) f(\mathbf{r}) \\ & \times e^{-i \int_0^t \omega(t-t_m) dt - i \mathbf{k}_m \mathbf{r} + i \varphi_m(\mathbf{r})} + \text{H.c.}, \end{aligned} \quad (1)$$

where the light field amplitude and the carrier frequency are

$$\varepsilon(t - t_m) = \varepsilon_0 \text{sech}[\beta(t - t_m)], \quad (2)$$

$$\omega(t - t_m) = \omega_0 + \mu \beta \tanh[\beta(t - t_m)], \quad (3)$$

where  $\mu$  and  $\beta$  define the frequency sweep range and the pulse duration,  $f(\mathbf{r})$  characterizes spatial properties of the light field,  $\mathbf{e}_c$  is the polarization of control light fields,  $t_{1,2}$  are the time delays of the pulses ( $t_2 = t_1 + \tau$ ),  $\mathbf{k}_c$  is the wave vector of the fields ( $\mathbf{k}_c \perp \mathbf{z}$ ), and  $\varphi_{1,2}(\mathbf{r})$  are slowly varied phases.

CHS pulses make it possible to achieve a pulse area close to  $\pi$  in a wider spectral frequency range [56] of the inhomogeneously broadened line and at the same time never exceed  $\pi$  for either site of Tm ions characterized by different Rabi frequencies. Such control pulses proved their importance in the efficiency enhancement of the ROSE protocol implementation [21,27]. Control pulses were formed from the continuous-wave Tekhnoscan TIS-SF-777 Ti:Sp laser radiation by acousto-optic modulators (AOMs). Then after AOMs, CHS pulses were spatially filtered by single mode optical fibers.

The bottom and top faces of the  $Tm^{3+} : Y_3Al_5O_{12}$  crystal were glued to the cold finger plate of the cryostat ( $20 \times 20$  mm dimensions) and to the copper top plate ( $10 \times 4$  mm dimensions), respectively, using a conductive silver paste (Silberleitlack). Bottom and top copper plates were polished and

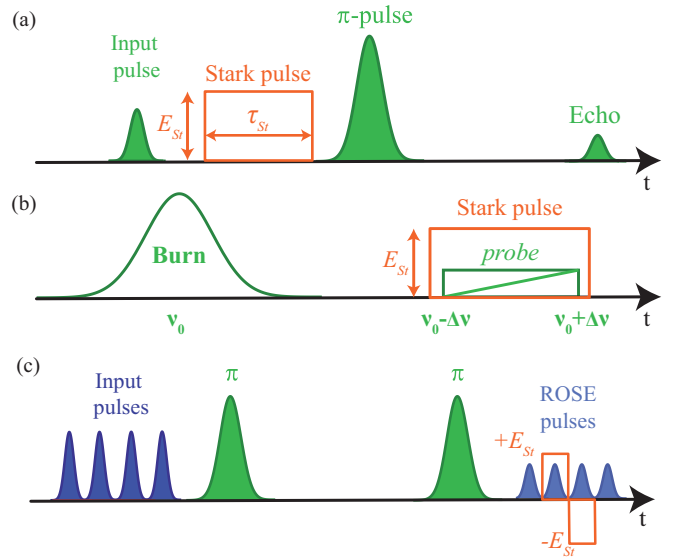


FIG. 2. Sequence of light pulses that were used to study the Stark effect in the  $Tm^{3+} : Y_3Al_5O_{12}$  crystal using (a) two-pulse photon echo, (b) spectral hole burning, and (c) ROSE protocol with the multipulse signal field using control Stark pulses of opposite polarities. Orange rectangles show the applied pulses of the external electric field. The pulses propagating in the control beam are shown in green and in the signal beam are shown by blue (as in Fig. 1).

used to produce the electric field pulses. Surface roughness of copper plates was  $\sim \lambda/2$ . The pulses were generated by an arbitrary waveform generator (BK Precision 4079B), then pre-amplified by an rf amplifier (Tabor Electronics A10160), and then finally passed through a high-voltage amplifier (Thorlabs HVA200). The resulting applied voltage range was  $\pm 200$  V. The distance between the top copper plate and the grounded cryostat cold finger was 2 mm (crystal thickness), which produced an electric field range of  $\pm 1$  kV/cm. The analysis of possible electric field inhomogeneities in the presented electrode circuit and their attachment to the sample is given in Sec. I in the Supplemental Material [50]. According to our estimations, the electric field inhomogeneity does not exceed 3.5% even for very strong defects in the surfaces of the crystal, electrodes, and glue.

### III. OBSERVATION OF LINEAR STARK EFFECT

Thulium ions in a  $Y_3Al_5O_{12}$  crystal replace yttrium ions in positions with the  $D_2$  point symmetry, meaning that a linear Stark effect is not expected. However, it can be sometimes observed in such systems when the symmetry of the ion position is broken due to the deformation in the local field around the ion [57]. In this section, we describe the first observation of the linear Stark effect in the  $Tm^{3+} : Y_3Al_5O_{12}$  crystal on the  ${}^3H_6(0) \rightarrow {}^3H_4(0)$  optical transition at the temperature 3.7 K.

This effect was studied by two techniques: two-pulse photon echo [Fig. 2(a)] and spectral hole burning [Fig. 2(b)]. We used only the control laser field (indicated in green in Fig. 1) propagating along the  $[\bar{1}10]$  crystallographic axis and polarized along the [110] axis of the  $Tm^{3+} : Y_3Al_5O_{12}$  crystal in both cases. In the first case, the amplitude ( $E_{St}$ ) and duration

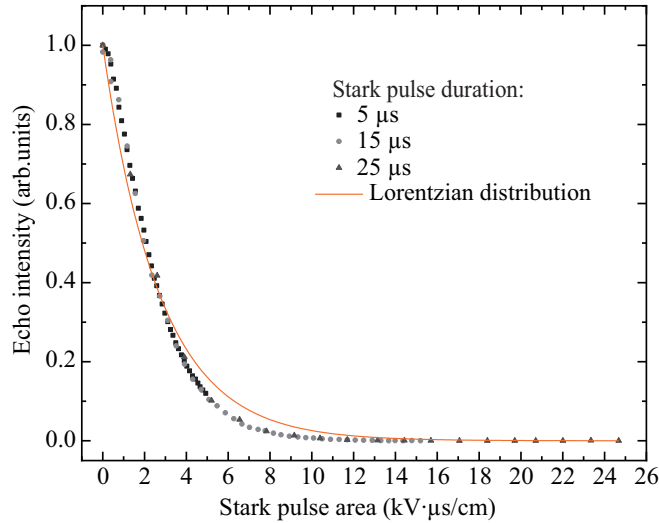


FIG. 3. Dependence of the two-pulse photon echo intensity on the Stark pulse area with different durations in the  $\text{Tm}^{3+} : \text{Y}_3\text{Al}_5\text{O}_{12}$  crystal on the  ${}^3\text{H}_6(0) \rightarrow {}^3\text{H}_4(0)$  transition at 3.7 K.  $E_{\text{laser}} \parallel E_{\text{St}} \parallel [110]$  the crystal axes. Squares, circles, and diamonds correspond to the Stark pulse duration of 5, 15, and 25  $\mu\text{s}$ , respectively. The orange curve is the theoretical fitting of the echo decay by the Lorentzian distribution of dipole moments characterized by the parameters  $\delta p_{0,L} = 65.2 \text{ Hz cm V}^{-1}$  corresponding to the full linewidth on half maximum.

( $\tau_{\text{St}}$ ) of the external electric field pulse were varied and the pulse was applied between the input signal and rephasing laser pulses. Figure 3 shows the dependence of the photon echo intensity on the area of the Stark pulse ( $S = E_{\text{St}} \tau_{\text{St}}$ ). Squares, circles, and diamonds represent three series of experiments with Stark pulse durations of  $\tau_{\text{St}} = 5 \mu\text{s}$ ,  $15 \mu\text{s}$ , and  $25 \mu\text{s}$ . It is seen in Fig. 3 that the echo signal did not recover at large values of the electric field pulse area  $S$ . When there are two types of ions acquiring opposite frequency shifts, the linear Stark effect leads to oscillating dependence of the echo pulse intensity on the electric pulse area  $S$  according to the formula

$$I_{\text{echo}} = \frac{1}{2} I_0 [1 + \cos(2\Omega \tau_{\text{St}})], \quad (4)$$

where  $I_0$  is the echo signal intensity when no field is applied,  $\Omega = p_0 E_{\text{St}}$ , and  $p_0$  and  $-p_0$  are dipole moments of two types of ions [58].

The absence of the echo signal recovery was observed earlier when the external geometric inhomogeneous electric dc Stark field (gradient electric field [29]) or ac Stark shift pulses [33,59] were used to implement the reversible inhomogeneous broadening technique combined with photon echo. In our case, we explain the echo signal suppression by attributing the linear Stark effect to the random lattice deformations or local perturbations of the crystal field around the  $\text{Tm}^{3+}$  ion sites that break the  $D_2$  symmetry.

To clarify the properties of this effect, we performed a spectral hole burning experiment. A spectral hole was burned by a long Gaussian shape pulse with a duration of 300  $\mu\text{s}$  (FWHM). After a time delay, a chirped pulse with the rectangular temporal shape (duration of 500  $\mu\text{s}$  and sweep range of 400 kHz) was used to read out the resulting spec-

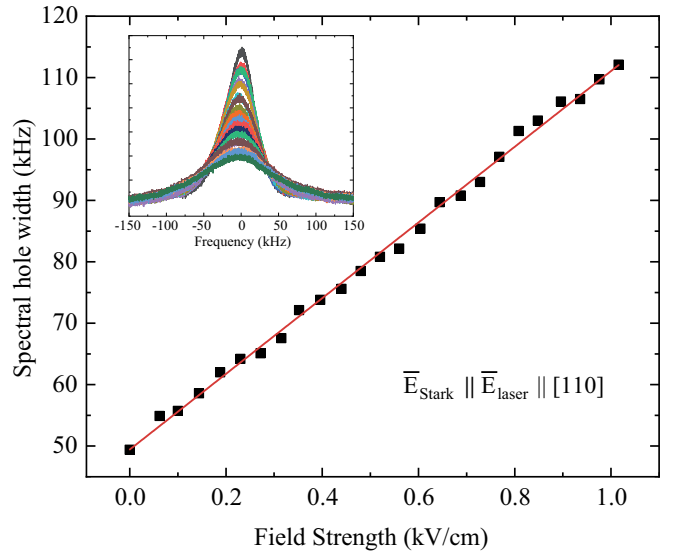


FIG. 4. Dependence of the width of the spectral hole  $\delta\nu_{\text{hom}}$  (kHz) on the  ${}^3\text{H}_6(0) \rightarrow {}^3\text{H}_4(0)$  transition of the  $\text{Tm}^{3+} : \text{Y}_3\text{Al}_5\text{O}_{12}$  crystal versus the external electric field strength  $E_{\text{St}}$  (kV/cm). The crystal was cooled down to  $T = 3.7 \text{ K}$ ,  $E_{\text{laser}} \parallel E_{\text{St}} \parallel [110]$  crystal axis. The red line is the linear fit of the experimental data according to the equation  $\delta\nu_{\text{hom}} = 49.4 + 61.6E_{\text{St}}$ . Inset: spectral hole broadening with the increase of the Stark field

tral hole of the Lorentzian shape with a full linewidth of  $\delta\nu_{\text{hom},0} = 49.4 \text{ kHz}$  [see Fig. 2(b)]. The time delay between centers of these pulses was 650  $\mu\text{s}$ . The external electric field pulse was applied during the readout. We performed a series of these experiments with different amplitudes of the external electric field  $E_{\text{St}}$  pulse. The inset in Fig. 4 shows that there is no splitting of the spectral hole; only the width of the hole increases linearly with the electric field amplitude. A small inhomogeneity of the electric field of  $\Delta E_{\text{St}} < \pm 3.5\%$  (see the Supplemental Material [50]) cannot cause the observed hole broadening and this experiment clearly shows the linearity of the Stark effect.

The obtained data (shown by squares in Fig. 4) are approximated well by the linear function  $\delta\nu_{\text{hom}}(\text{kHz}) = 49.4 + 61.6E_{\text{St}}$ . This gives us the coefficient  $\delta p_0 = 61.6 \pm 0.5 \text{ Hz cm V}^{-1}$  that characterizes the linear growth of the linewidth  $\delta\nu_{\text{hom}}$  with the amplitude of the applied electric field  $E_{\text{St}}$ , which also indicates the distribution in the coefficient of the linear Stark effect in the ion system. In this case, each  $j$ th thulium ion in the ensemble has its own effective dipole moment  $\delta p_j$  and frequency shift produced by the external electric field  $\Omega_j = \delta p_j E_{\text{St}}$ . Accordingly, in our experimental data, we have a smooth distribution  $G(\delta p)$  of the dipole moments  $\delta p$ , which is almost symmetric with respect to zero. For the theoretical estimation, we apply Lorentzian  $\frac{\delta p_{0,L}/2}{\pi(\delta p^2 + \delta p_{0,L}^2/4)}$  distribution with the dipole moment  $|\delta p_{0,L}/2|$  on half maximum, which is similar but does not completely coincide with the experimental distribution of  $G(\delta p)$  (see Fig. 3). Unlike [58], where the echo oscillations are described by the presence of only two dipole moments [see Eq. (4)], in our case, the observed echo decayed steadily (see Fig. 3) due to the destructive interference of the polarization of excited



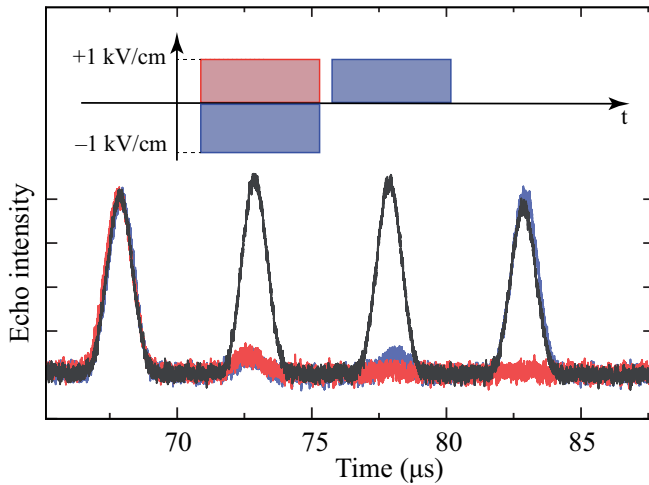


FIG. 5. Lower panel demonstrates four ROSE signals in the case of four input pulses in the  $\text{Tm}^{3+} : \text{Y}_3\text{Al}_5\text{O}_{12}$  crystal on the  ${}^3\text{H}_6(0) \rightarrow {}^3\text{H}_4(0)$  transition at 3.7 K. The upper panel shows the applied voltage during the revival of second and third silenced echo pulses. The second and third pulses are partially suppressed by the external electric field pulses with the opposite polarity (blue line), but the fourth pulse has approximately the same amplitude (blue solid line) as the echo pulse in the absence of the external electric field (black solid line). The red solid line demonstrates the suppression of all echo pulses after 70  $\mu\text{s}$ .

ions with a continuous distribution of the ion frequency shifts  $\Omega(\delta p) = \delta p E_{st}$ . For Lorentzian distribution, the echo decay is  $\sim \exp\{-\delta p_{0,L} E_{st} \tau\}$  that gives  $\delta p_{0,L} = 65.2 \text{ Hz cm V}^{-1}$ , which, with small deviations from the experimental data, well describes the behavior of the echo over a wide range of Stark pulse area (see Fig. 3). The estimated value  $\delta p_{0,L} = 65.2$  is sufficiently close to the value  $\delta p_0 = 61.6$  experimentally measured from the dependence of the spectral hole width; see Fig. 4. The linear dependence of the hole burning linewidth  $\delta\nu_{\text{hom}}$  on the electric field  $E_{st}$  in Fig. 4 is also in good agreement with the linear Stark effect and Lorentzian character of the dipole moment distribution  $G(\delta p)$  determining a similar behavior of linewidth  $\delta\nu_{\text{hom}} = \delta\nu_{\text{hom},0} + \delta p_{0,L} E_{st}$ .

At the same time, we have to note that the distribution  $G(\delta p)$  in our  $\text{Tm}^{3+} : \text{Y}_3\text{Al}_5\text{O}_{12}$  crystal has a more complex structure than pure Lorentzian distribution. The studies of the observed linear Stark effect in connection with the features of its local inhomogeneity in several  $\text{Tm}^{3+} : \text{Y}_3\text{Al}_5\text{O}_{12}$  crystals and orientations of the external electric field versus crystallographic axes could be a subject of further more detailed investigations based on the use of theoretical approaches to the description of the physical properties of random local inhomogeneities of the crystal lattice and their influence on the spectroscopic parameters of the REIs [60,61].

To understand the possible usage of the observed Stark effect in multiqubit QM, we stored four weak signal pulses in the cavity-assisted ROSE memory protocol. Figure 2(c) shows the sequence of light pulses used in this experiment. Four retrieved light echo signals are shown in Fig. 5. We observed that the external electric field pulse applied at the time of the second echo signal emission (red curve in Fig. 5) suppresses subsequent echo signals at  $t \approx 78 \mu\text{s}$  and  $t \approx 83 \mu\text{s}$ . However,

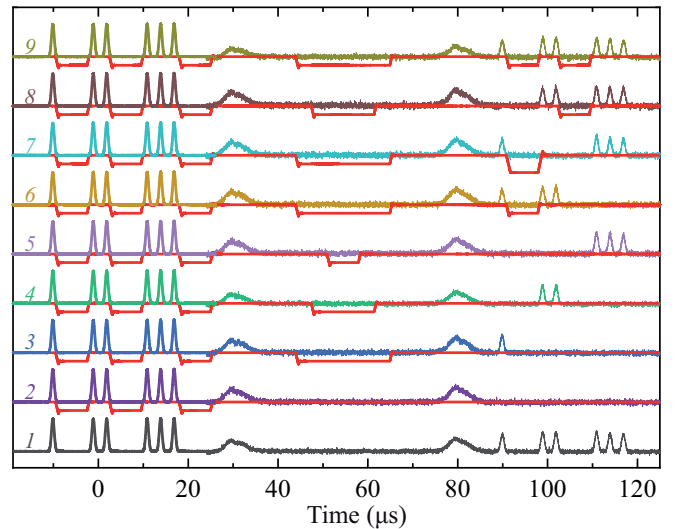


FIG. 6. Addressable readout of the input optical signals by using Stark pulses in the ROSE memory scheme in the  $\text{Tm}^{3+} : \text{Y}_3\text{Al}_5\text{O}_{12}$  crystal placed into an optical cavity. In all cases, three groups of the input pulses are sent to the memory cell. The incident signal light pulses before the cavity, which are reduced by a factor of 100, are shown at  $t = 0$ . Signals from the second detector are plotted for  $t > 25 \mu\text{s}$ . Signals from the control pulses can be seen at  $t = 30 \mu\text{s}$  and  $t = 80 \mu\text{s}$ . The lower (gray) curve shows the recovery of all the input pulses without the external electrical field pulses. The remaining curves correspond to the suppression of all the reading signals, individual signals, pairs of signals, and recovery of all the recorded light pulses. Red curves show the external electric field pulses for each series.

if we apply the additional electric field pulse of the same area  $S$ , but with the opposite polarity, the echo signal (at  $t \approx 83 \mu\text{s}$ ) is restored (blue curve in Fig. 5). The external electric field weakly affects the intensity and temporal shape of the restored echo signal (black and blue curves in Fig. 5). Here we used the measure of the echo recovery efficiency (or addressing efficiency for Sec. IV)  $\eta_{\text{adr}} = 1 - \frac{|I - I_{\text{Stark}}|}{I}$ , where  $I_{\text{Stark}}$  and  $I$  are the echo pulse intensities with and without the action of the two electric pulses of the opposite polarity. For this and the following experiments (Sec. IV) the measured value  $\eta_{\text{adr}} = 95 \pm 1\%$  showed a high addressing efficiency.

#### IV. ADDRESSABLE STORAGE OF THE SIGNAL PULSES IN ROSE PROTOCOL

Below we use the properties of the observed Stark effect in the  $\text{Tm}^{3+} : \text{Y}_3\text{Al}_5\text{O}_{12}$  crystal for the implementation of addressable writing and readout of multipulse light fields. The proposed protocol is based on the temporal encoding of the original input signals with its retrieval by choosing the appropriate area  $S$  of the additional encoding Stark pulses controlling the dephasing and phasing of the excited optical coherence of thulium ions.

Figure 6 shows the encoding cases with various combinations of electric pulses and their compensating counterparts in writing and reading processes. The experimental setup was that shown in Fig. 1 where SPCM and TDC in the signal field path are replaced by the avalanche photodetector

(Thorlabs 120A/M) and oscilloscope (Tektronix DPO7104C), respectively. In all the cases, three groups of input weak optical pulses were launched to the memory cell ( $\text{Tm}^{3+} : \text{Y}_3\text{Al}_5\text{O}_{12}$  crystal): single, double, and triple pulses in the first, second, and third groups, respectively. The lowest gray (1) curve in Fig. 6 shows the recovery of all the input pulses without external Stark pulses characterized by the retrieval efficiency of 0.5% and storage time of 100  $\mu\text{s}$ . Then a Stark pulse was applied with a duration of 7  $\mu\text{s}$  and electric field strength of 1 kV/cm (with pulse area  $S$ ) after each group of the input signal fields. In this case, all the ROSE echo signals are suppressed as shown by the purple (2) curve in Fig. 6. It can be seen in Fig. 3 that the echo is suppressed by a factor of 30 using a single Stark pulse. At the same time, the usage of two such Stark pulses leads to the suppression of the echo pulse by three orders of magnitude. For example, in comparison between the traces 1 and 2 in Fig. 6, the second group (double pulses) is suppressed by more than three orders of magnitude and the third group (triple pulses) is suppressed in 30 times.

To successfully read out the desired input signal, it is necessary to apply an electric pulse after the first or second control optical  $\pi$  pulse of such area  $S$  that compensates the additional dephasing of thulium ions caused by encoding Stark pulses. In the assumption there is no atomic decoherence, the maximum number of addressable input pulses ( $N$ ) is limited by the maximum applicable field strength ( $E_{\text{St,max}}$ ) and the delay between the rephasing pulses ( $\tau$ ) to successfully read any ROSE echo pulse. These conditions must be fulfilled simultaneously and can be written as follows:  $N \leq E_{\text{St,max}}/E_{\text{St}}$  and  $N \leq \tau/(\tau_{\text{inp}} + \tau_{\text{St}})$ , where  $\tau_{\text{inp}}$  is the duration of a single input light pulse and  $\tau$  is the delay between the rephasing pulses. The blue (3) graph shows the selective readout of a single pulse from the first group with an external electric field with an area of  $3S$  applied between the two  $\pi$  pulses, while the second and third pulse groups are not recovered. In the same way, double and triple light pulses are read out by applying the electric pulses with  $2S$  and  $S$  areas between the two rephasing pulses—green (4) and light purple (5) graph, respectively. The remaining graphs (6)–(8) in Fig. 6 demonstrate the pairwise readout of the input light pulses and the recovery of all the input light pulses as shown in the upper (9) curve. As it was mentioned in the previous section, the addressing efficiency in this experiment was also  $\eta_{\text{adr}} = 95 \pm 1\%$ .

We note that the same group of pulses can be selectively read out by different time sequences of the external electric Stark pulses, as long as it fully compensates the accumulated dephasing for the each group of the signal pulses. Moreover, by applying additional rephasing laser  $\pi$  pulses, we can recall the signal pulse sequences out of the initial temporal order as it is shown in Fig. 7. In this case, the storage time was 80  $\mu\text{s}$  and retrieval efficiency was about 5% in the first recall window (from  $t = 80 \mu\text{s}$  to  $t = 100 \mu\text{s}$ ) and about 0.3% in the second recall window (from  $t = 160 \mu\text{s}$  to  $t = 180 \mu\text{s}$ ). Different efficiencies of the recalled ROSE pulses in our experiment were determined by the finite phase relaxation time of the atomic transition and by the deviation of the pulse area of the optical rephasing pulses from  $\pi$ . The use of even shorter signal light pulses and more accurate control  $\pi$ -pulse tuning can significantly increase the efficiency of the signal

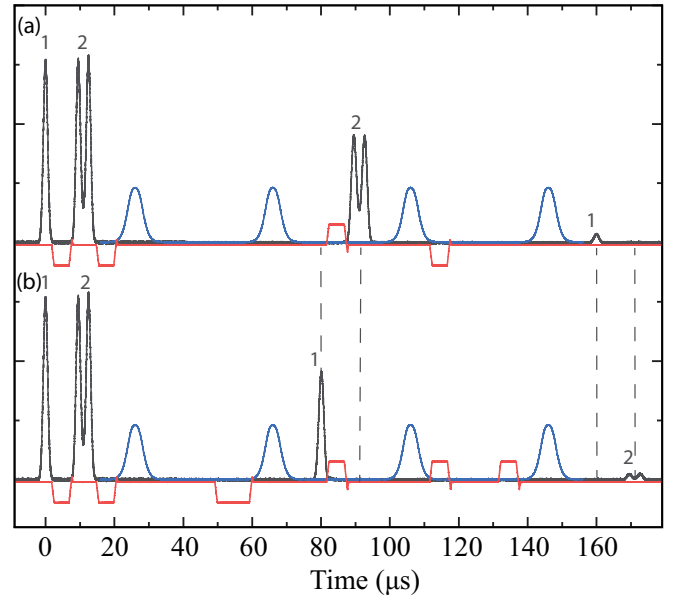


FIG. 7. Experimental results on recall of light sequence with (a) reversed and (b) original temporal order (black curves). The reflected part of the input pulse (about  $\sim 8\%$ ) from the cavity due to mismatching is shown at  $t = 0 \mu\text{s}$ . The chosen recall order is controlled by the number and polarities of external electric field pulses (red curves). Optical rephasing pulses (control beam) are shown by blue. Different intensities of the recalled ROSE pulses in our experiments were determined mainly by the phase relaxation  $T_M$  of atomic transition.

pulse readout in the addressing regime in the crystal under study.

The implementation of addressable writing and readout of multipulse signal light fields was possible in our experiments due to the distribution of the linear Stark coefficients inside the ensemble of thulium ions in the  $\text{Y}_3\text{Al}_5\text{O}_{12}$  crystal. Such an addressing scheme could also be achieved in crystals with the uniform linear Stark effect using external electric field gradient as was originally described in [62,63].

## V. CAVITY-ASSISTED ROSE PROTOCOL AT FEW PHOTON LEVEL

In this section, we present experimental implementation of an optical storage of a few photon signal pulse in the cavity-assisted ROSE protocol under the impedance-matching condition. Then we discuss the obtained results and possible ways to further improve this protocol.

Coming back to the main requirements for the perfect implementation of the ROSE protocol, we note that using ideal controlled laser  $\pi$  pulses is not enough, but is one of the important conditions. In particular, for collinear signal and control light field propagation geometries, strong rephasing laser pulses remain a potential noise source due to the appearance of spontaneous emission during the echo signal caused by rephasing of the amplified spontaneous emission [28]. In this respect, the transverse (orthogonal) geometry of the light beams used in this work seems to be preferable, since it does not cause the rephased amplified spontaneous emission [28]

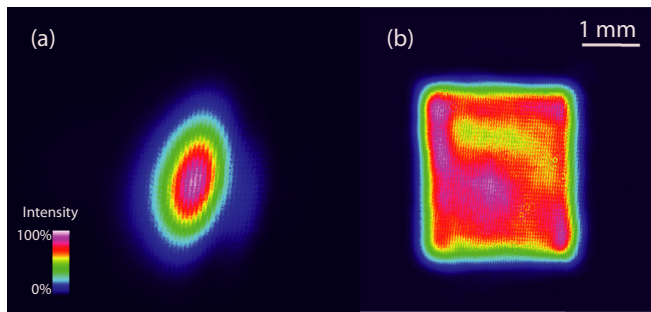


FIG. 8. Laser beam profile of the control field in the case of (a) Gaussian beam and (b) so-called top hat shape, after the GTH lens.

due to phase mismatching ( $|2k_c \pm ke_z| \neq k$ ). The transverse geometry also provides a sufficiently good spatial isolation between the optical paths of the signal and control fields. Still, the perfect signal retrieval requires ideal rephasing pulses, which are difficult to implement experimentally. Here we apply several techniques to improve the quality of the rephasing control.

First, a Gauss to top hat lens (Eksma Optics GTH-3.6-1.75FA-NIR; see Fig. 1) was applied to the control laser beam that transforms the beam profile to minimize the variations of its intensity in the beam cross section (see Fig. 8). Second, a series of filters were added to the signal beam detection path as in [22]. A fluorescence bandpass filter (Edmund Optics 84106) was added in the signal field beam (indicated by the letter  $F$  in Fig. 1). It blocked luminescence from  ${}^3\text{H}_6(0)$  to the excited sublevels  ${}^3\text{H}_4(n > 0)$  of the ground multiplet of thulium ions. A Glan-Taylor polarizer filtered orthogonally polarized light fields. These filters together reduced quantum noise caused by the luminescence in our experiment by more than 20 times. For the broadband efficient coherent control of the atomic coherence in both atomic groups with different dipole moment orientations, we used the two CHS pulses with parameters  $\beta = 70$  kHz and  $\mu = 3.5$  [see Eq. (2) and Eq. (3)] resulting in the 490 kHz sweep interval. These improvements reduced the level of optical quantum noise after two rephasing laser pulses to about one photon in the  $2 \mu\text{s}$  time interval. All the optical elements in the signal field path were AR coated. After passing through these optical elements, the retrieved echo signal was launched to the single photon counting module (SPCM, Excelitas SPCM-AQRH) through the single mode fiber and then measured by a time-to-digital converter (TDC, IDQ ID-801) or an oscilloscope (Tektronix DPO 7104C).

Figure 9 shows the experimental data of the optical storage of the weak input light pulse obtained in the ROSE protocol in the impedance-matched optical cavity. The input signal light pulse (blue curve in Fig. 9) in the coherent state was launched at  $t = 0$  with an average of  $5.6 \pm 0.1$  photons per pulse and had a Gaussian temporal shape with a  $2 \mu\text{s}$  duration (FWHM). The curve with the input pulse was measured by SPCM1 in Fig. 1. At the time 10 and  $26 \mu\text{s}$  luminescence signals from 2 CHS pulses were detected by SPCM1 caused by the ghost image of the beam splitter and the absence of the fluorescence filter and the Glan-Taylor polarizer in this path. Each curve in Fig. 9 is obtained by integrating 3000 ROSE

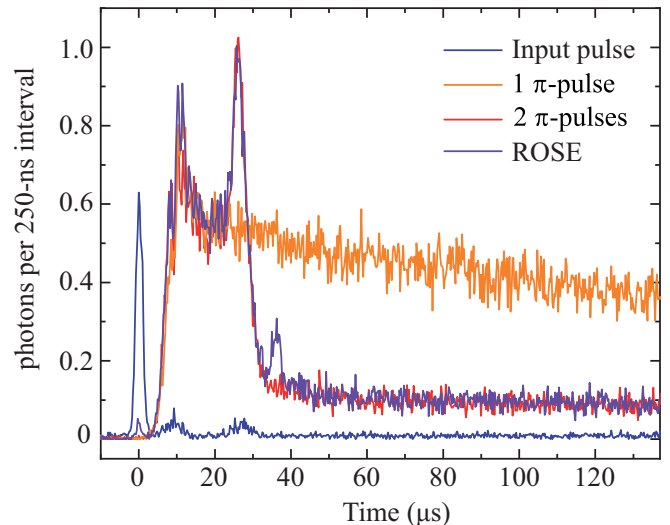


FIG. 9. Storage and retrieval of few photon signals in the ROSE scheme with the  $\text{Tm}^{3+} : \text{Y}_3\text{Al}_5\text{O}_{12}$  crystal placed into the impedance-matched optical cavity. Input pulse (blue curve at  $t = 0 \mu\text{s}$ ) contains  $\bar{n} = 5.6$  photons on average. At the time  $t = 36 \mu\text{s}$  the violet curve represents the ROSE signal with the retrieval efficiency of  $\eta = 27 \pm 2\%$ . The orange curve represents the signal after applying only one rephasing pulse at  $t = 9 \mu\text{s}$  and the red curve represents the signal after applying two rephasing pulses at  $t = 9 \mu\text{s}$  and  $t = 27 \mu\text{s}$  without the input pulse.

protocol sequences with the 1 Hz repetition rate corresponding to 50 min data collection time. Further, we normalized the overall detection efficiency by taking into account the SPCM efficiency (65%) detection and the losses in the signal field detection path after the beam splitter to SPCM2 (62%).

A part of the input signal pulse (about  $\sim 8\%$ ) was reflected (the violet curve at  $t = 0 \mu\text{s}$  in Fig. 9) and detected by SPCM2. In our opinion, reflection is caused by mismatching of the transverse spatial Gaussian mode of the signal field with the light mode of the concentric resonator. The rest of the input signal field is absorbed in the cavity and slightly scattered. Details of estimations of intracavity losses and rephasing efficiency by the control laser pulses are presented in the Supplemental Material [50].

We consider the violet curve in Fig. 9 that corresponds to the signal obtained by SPCM2. At the time of 10 and  $26 \mu\text{s}$ , quite intense signals caused by luminescence from two CHS pulses are also visible. At  $t = 36 \mu\text{s}$  the ROSE echo signal is emitted with the retrieval efficiency of  $\eta = 27 \pm 2\%$ . The signal at  $t > 36 \mu\text{s}$  corresponds to the long tail of atomic emission due to the luminescence from the  ${}^3\text{H}_6(0)$  excited optical level with the lifetime of  $T_1 = 550 \pm 20 \mu\text{s}$ , which is close to the values obtained in [22,64].

The storage of the signal light pulse with  $\bar{n}_{\text{signal}} = 5.6$  photons on average leads to the ROSE echo signal containing  $\bar{n}_{\text{echo}} = 1.6 \pm 0.1$  photons on average (violet curve in Fig. 9), which was comparable with the optical noise level of 1.2 photon after Gaussian averaging within the echo temporal mode (red curve in Fig. 9). Thus the developed cavity-assisted ROSE protocol provided the reduction of the level of the input signal pulse in more than  $\sim 2.5$  times in comparison with the

free space ROSE scheme [22] (14 photons on average) for the similar signal-to-noise ratio. It is worth noting that the authors of [22] used the collinear counterpropagating geometry where the signal field is cross-polarized with respect to the rephasing laser pulse. They deflect stray light from the rephasing pulses by polarizer pairs which offer a nominal extinction ratio of  $10^{-7}$ . In this work, the polarizations of signal and rephasing light beams were the same; instead we used the spatial isolation of the signal field, provided by the orthogonal geometry. Thus, comparing our results with those of [22], we can say that the isolation is better than  $10^{-7}$ . Moreover, two control laser pulses in the orthogonal geometry do not generate a spurious two-pulse echo near the ROSE echo, as they do in counterpropagating geometry [22]. These properties of the orthogonal control scheme, together with the absence of rephased amplified spontaneous emission [28] and doubling the retrieval efficiency, make it particularly advantageous.

To analyze the achieved efficiency of ROSE echo emission, we use the photon echo pulse area approach developed in our previous works [65–67]. In our case, it is viable, since the input signal pulse spectrum is much narrower than the inhomogeneous broadening of the atomic transition and cavity mode linewidth. Under this condition, the retrieved echo pulse reproduces the temporal shape of the signal pulse, as we observe in our experiments (see Fig. 6). This makes it possible to estimate the energy efficiency as  $\eta = n_{\text{echo}}/n_{\text{signal}} \cong (\Theta_{\text{echo}}/\Theta_{\text{signal}})^2$  for the weak input signal pulse with a small pulse area  $\Theta_{\text{signal}} \ll 1$ . By assuming that both control pulses are identical, we can write the formula for the energy efficiency:

$$E = \left( \frac{4 e^{-(2\tau/T_M)^x} \sum_m \tilde{z}_m \langle \sin^4(\frac{\Theta_m(\mathbf{r}_\perp)}{2}) \rangle}{(1 + \tilde{\gamma} + \tilde{z}) [1 + \tilde{\gamma} + \sum_m \tilde{z}_m \langle w_m(4\tau, \mathbf{r}_\perp) \rangle]} \right)^2. \quad (5)$$

In this analytical solution, we take into account that there are two groups of atoms with different concentrations and dipole moment projections  $d_m$ ; hence the index  $m = 1, 2$  for  $\tilde{z}_m = 2\pi\alpha_{0m}l/\kappa$ ,  $w_m$ ,  $\Theta_m = (2d_m/\hbar) \int E(t, \mathbf{r}) dt$ ,  $\kappa$  is the coupling constant between the light field and the cavity mode,  $\tilde{\gamma} = \gamma/\kappa$  are normalized cavity losses,  $\tau$  is the delay between rephasing pulses, and  $T_M$  is phase-memory time with parameter  $x$ . These parameters can be determined from the experiment:  $\tilde{\gamma} = (1 - \sqrt{r_0})/(1 + \sqrt{r_0})$ , here  $r_0$  is the cavity reflection coefficient outside the  $\text{Tm}^{3+}$  absorption line, and  $\tilde{z} = [1 - \tilde{\gamma} - (1 + \tilde{\gamma})\sqrt{r_1}]/(1 + \sqrt{r_1})$ , where  $r_1$  is the leftover cavity reflection coefficient under the impedance matching condition. In our experiments we have  $r_0 = 0.75$ ,  $r_1 = 0.08$ , so  $\tilde{\gamma} = 0.072$ ,  $\tilde{z}_1 = 0.49$ .

We also take into account the transverse spatial inhomogeneity of the control pulses where we can ignore changes of these pulse areas due to the interaction with the resonant transition. By taking into account  $\Theta_m(\mathbf{r}_\perp) = \Theta_m + \delta\Theta_m(\mathbf{r}_\perp)$  in the solution, we average the atomic response over  $\mathbf{r}_\perp$ , denoted as  $\langle \dots \rangle$  in Eq. (5). For the frequency chirped pulses we estimate the pulse area of the control pulses by the created inversion after the propagation of the pulse:  $w_m = -\cos \Theta_m$ . So the fact that  $\Theta_m(\mathbf{r}_\perp)$  depends on  $\mathbf{r}_\perp$  means that  $w_m$  also depends on  $\mathbf{r}_\perp$  and we need to average it as well. The full expression for  $w_m$  as well as other details of the derivation of Eq. (5) can be found in the Supplemental Material [50].

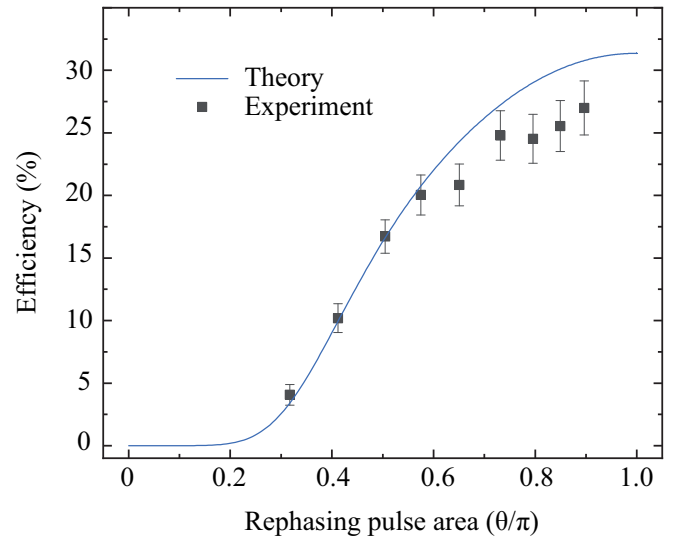


FIG. 10. Experimental (black squares) and theoretical (blue solid curve) dependence of the ROSE echo efficiency versus the pulse area of the two identical rephasing laser pulses. The theoretical curve corresponds to Eq. (5). Values on the  $x$  axis correspond to the weakly interacting group of atoms so  $\theta = \Theta_1$  (see text for details).

Figure 10 shows the comparison between the experimental data and the analytical solution Eq. (5). To obtain the data, we simultaneously varied the amplitudes of the rephasing laser pulses and measured the resulting echo retrieval efficiency. In this case, we used bright signal pulses and SPCMs were replaced by APDs. The observed slight disagreement can be associated with the different efficiencies for single-shot and averaging mode (see Supplemental Material [50]), the finiteness of the optical density of the resonant transition, and, possibly, some other simplifications of the model used, requiring further refinement.

The study of noise at the ROSE echo emission time is an important issue of the QM scheme deserving a separate dedicated research; here we present only our initial observations on this matter. After the second CHS pulse (red curve in Fig. 9) the luminescence tail caused by spontaneous emission is about four times smaller than after a single CHS pulse (orange curve in Fig. 9). Both curves are obtained without the input signal pulse and detected by SPCM2. A significant increase in the decay rate of the excited optical level between the rephasing laser pulses was also observed, which can be associated with the amplification of spontaneous emission in the optical cavity. For example, after applying only one rephasing laser pulse (orange curve in Fig. 9), the effective lifetime of ions emitting into the cavity mode decreases from  $T_1 = 550 \pm 20 \mu\text{s}$  to  $T_1 = 250 \pm 10 \mu\text{s}$ . Accelerated luminescence itself is one of the sources of optical quantum noise. The luminescence increases the extra population of excited atomic states at the time of ROSE echo emission leading to the optical noise amplification. However this effect can be eliminated by using a cavity with a switched frequency and/or its quality factor. A deeper understanding of the properties of the observed optical noise requires a detailed study of the spectral properties of the excited atoms and the kinetics of their decay in the cavity, which is the subject of a special theoretical study



based on the use of a rigorous quantum approach to studying the QM protocol.

## VI. CONCLUSION

In this work, we observed the linear Stark effect in the  $\text{Tm}^{3+} : \text{Y}_3\text{Al}_5\text{O}_{12}$  crystal and explained it by the perturbations of the crystal field around the  $\text{Tm}^{3+}$  ion sites that break the local  $D_2$  symmetry of the used crystal. Using this effect, we implemented addressable optical memory in this crystal for the weak multipulse light fields in the impedance-matched cavity-assisted photon echo ROSE protocol. The protocol featured highly efficient addressing (>95%) of the input light pulses.

We also show that the cavity-assisted ROSE memory scheme demonstrates larger efficiency for the storage of few photon fields in comparison with the previous experiments on the ROSE protocol in the free space configuration [22]. The developed memory scheme was implemented for the lower optical depth (0.125) of the atomic transition and smaller average number of photons (5.6 photons) in the input signal light pulse, that is more than twice reduced in comparison with 14 photons in the free space configuration [22] for the same signal-to-noise ratio of 1 in the retrieved light pulse.

In addition, the analysis of the results showed that the implemented cavity-assisted QM scheme can be considerably improved in its basic parameters including the significant decrease in optical quantum noise. Here, we can note two main directions of future works. First, the quality improvement of the  $\pi$  pulses could slightly increase efficiency and significantly reduce noise. This seems to be practically possible in CHS pulse shaping techniques using the high-precision amplitude-frequency modulation of a coherent laser radiation with sufficiently high intensity. Using such CHS pulses increases the spectral range of the perfect coherent atomic control, the efficiency of the QM protocol, and decreases the level of spontaneous emission during echo signal emission. It is worth noting that the solution to the problem of nonideal optical  $\pi$  pulses is important in itself in such fields as the

efficient transfer of atomic coherence from the optical range to the microwave one, the improvement of the Raman QM protocols, creation of broadband QM schemes, and in other fields of quantum processing. For a more precise control of the geometric shape of the wave front of the rephasing laser field, a spatial light modulator can be useful, which is widely used, e.g., to prepare light with an orbital angular momentum.

Secondly, we can also apply one more important resource for the reduction of the quantum noise level after the action of the first control laser field. Namely, we can dynamically reduce (and recover) the quality factor and/or change the resonant frequency of the used cavity before the first control laser  $\pi$  pulse and then bring it back after the second  $\pi$  pulse. This procedure drastically suppresses the level of atomic luminescence between the two control laser pulses and undesirable optical noise.

Finally, the signal-to-noise ratio can be improved by increasing the efficiency of the QM by using REI-doped crystals with the longer optical coherence time and lifetime of the excited state, like in  $\text{Tm}^{3+} : \text{Y}_3\text{Ga}_5\text{O}_{12}$  [18],  $\text{Eu}^{3+} : \text{Y}_2\text{SiO}_5$  [68], and  $\text{Er}^{3+} : \text{Y}_2\text{SiO}_5$  [23,69] crystals, where the QM scheme could provide the visible storage of single photon pulses. A considerable increase in the efficiency can be also obtained by using another type of actively developed resonators (microresonators and nanophotonic resonators) and by achieving better matching of the cavity mode with the input field (e.g., confocal type); it is also necessary to minimize spurious losses inside the cavity by finer-tuning and using better quality mirrors and antireflection coatings.

The solution of the above complex of physical and technical tasks will undoubtedly lead to the implementation of the ROSE protocol with the lower noise level applicable for the quantum storage of single photon fields. This work is an important step towards solving these problems.

## ACKNOWLEDGMENTS

This research was supported in part by the Ministry of Science and Higher Education of the Russian Federation (Project No. 14.Z50.31.0040).

- 
- [1] A. I. Lvovsky, B. C. Sanders, and W. Tittel, Optical quantum memory, *Nat. Photon.* **3**, 706 (2009).
  - [2] F. Bussi eres, N. Sangouard, M. Afzelius, H. de Riedmatten, C. Simon, and W. Tittel, Prospective applications of optical quantum memories, *J. Mod. Opt.* **60**, 1519 (2013).
  - [3] K. Heshami, D. G. England, P. C. Humphreys, P. J. Bustard, V. M. Acosta, J. Nunn, and B. J. Sussman, Quantum memories: emerging applications and recent advances, *J. Mod. Opt.* **63**, 2005 (2016).
  - [4] T. Chaneli ere, G. H etet, and N. Sangouard, Quantum optical memory protocols in atomic ensembles, *Advances in Atomic, Molecular and Optical Physics* (Academic Press, New York, 2018), Vol. 67, pp. 77–150.
  - [5] H. J. Kimble, The quantum internet, *Nature (London)* **453**, 1023 (2008).
  - [6] N. Sangouard, C. Simon, H. de Riedmatten, and N. Gisin, Quantum repeaters based on atomic ensembles and linear optics, *Rev. Mod. Phys.* **83**, 33 (2011).
  - [7] W. Tittel, M. Afzelius, T. Chaneli ere, R. Cone, S. Kr oll, S. Moiseev, and M. Sellars, Photon-echo quantum memory in solid state systems, *Laser Photon. Rev.* **4**, 244 (2009).
  - [8] S. A. Moiseev and S. Kr oll, Complete Reconstruction of the Quantum State of a Single-Photon Wave Packet Absorbed by a Doppler-Broadened Transition, *Phys. Rev. Lett.* **87**, 173601 (2001).
  - [9] M. Bonarota, J.-L. Le Gou et, and T. Chaneli ere, Highly multimode storage in a crystal, *New J. Phys.* **13**, 013013 (2011).
  - [10] R. M. Macfarlane, High-resolution laser spectroscopy of rare-earth doped insulators: a personal perspective, *J. Lumin.* **100**, 1 (2002).
  - [11] N. Kunkel and P. Goldner, Recent advances in rare earth doped inorganic crystalline materials for quantum information processing, *Z. Anorg. Allg. Chem.* **644**, 66 (2017).
  - [12] M. Zhong, M. P. Hedges, R. L. Ahlefeldt, J. G. Bartholomew, S. E. Beavan, S. M. Wittig, J. J. Longdell, and M. J. Sellars,

- Optically addressable nuclear spins in a solid with a six-hour coherence time, *Nature (London)* **517**, 177 (2015).
- [13] M. Rančić, M. P. Hedges, R. L. Ahlefeldt, and M. J. Sellars, Coherence time of over a second in a telecom-compatible quantum memory storage material, *Nature Phys.* **14**, 50 (2018).
- [14] A. Ortu, A. Tiranov, S. Welinski, F. Fröwis, N. Gisin, A. Ferrier, P. Goldner, and M. Afzelius, Simultaneous coherence enhancement of optical and microwave transitions in solid-state electronic spins, *Nat. Mater.* **17**, 671 (2018).
- [15] R. M. Macfarlane, Photon-echo measurements on the trivalent thulium ion, *Opt. Lett.* **18**, 1958 (1993).
- [16] C. W. Thiel, N. Sinclair, W. Tittel, and R. L. Cone, Optical decoherence studies of Tm<sup>3+</sup>: Y<sub>3</sub>Ga<sub>5</sub>O<sub>12</sub>, *Phys. Rev. B* **90**, 214301 (2014).
- [17] C. W. Thiel, R. M. Macfarlane, Y. Sun, T. Böttger, N. Sinclair, W. Tittel, and R. L. Cone, Measuring and analyzing excitation-induced decoherence in rare-earth-doped optical materials, *Laser Phys.* **24**, 106002 (2014).
- [18] C. W. Thiel, N. Sinclair, W. Tittel, and R. L. Cone, Tm<sup>3+</sup>: Y<sub>3</sub>Ga<sub>5</sub>O<sub>12</sub> Materials for Spectrally Multiplexed Quantum Memories, *Phys. Rev. Lett.* **113**, 160501 (2014).
- [19] T. Chanelière, M. Bonarota, V. Damon, R. Lauro, J. Ruggiero, I. Lorgère, and J.-L. Le Gouët, Light storage protocols in Tm:YAG, *J. Lumin.* **130**, 1572 (2010).
- [20] J. H. Davidson, P. Lefebvre, J. Zhang, D. Oblak, and W. Tittel, Improved light-matter interaction for storage of quantum states of light in a thulium-doped crystal cavity, *Phys. Rev. A* **101**, 042333 (2020).
- [21] V. Damon, M. Bonarota, A. Louchet-Chauvet, T. Chanelière, and J.-L. Le Gouët, Revival of silenced echo and quantum memory for light, *New J. Phys.* **13**, 093031 (2011).
- [22] M. Bonarota, J. Dajczgewand, A. Louchet-Chauvet, J.-L. Le Gouët, and T. Chanelière, Photon echo with a few photons in two-level atoms, *Laser Phys.* **24**, 094003 (2014).
- [23] J. Dajczgewand, J.-L. Le Gouët, A. Louchet-Chauvet, and T. Chanelière, Large efficiency at telecom wavelength for optical quantum memories, *Opt. Lett.* **39**, 2711 (2014).
- [24] B. Julsgaard, C. Grezes, P. Bertet, and K. Mølmer, Quantum Memory for Microwave Photons in an Inhomogeneously Broadened Spin Ensemble, *Phys. Rev. Lett.* **110**, 250503 (2013).
- [25] M. Nilsson and S. Kröll, Solid state quantum memory using complete absorption and re-emission of photons by tailored and externally controlled inhomogeneous absorption profiles, *Opt. Commun.* **247**, 393 (2005).
- [26] J. Dajczgewand, R. Ahlefeldt, T. Böttger, A. Louchet-Chauvet, J.-L. Le Gouët, and T. Chanelière, Optical memory bandwidth and multiplexing capacity in the erbium telecommunication window, *New J. Phys.* **17**, 023031 (2015).
- [27] K. I. Gerasimov, M. M. Minnegaliev, S. A. Moiseev, R. V. Urmancheev, T. Chanelière, and A. Louchet-Chauvet, Quantum memory in an orthogonal geometry of silenced echo retrieval, *Opt. Spectrosc.* **123**, 211 (2017).
- [28] P. M. Ledingham, W. R. Naylor, J. J. Longdell, S. E. Beavan, and M. J. Sellars, Nonclassical photon streams using rephased amplified spontaneous emission, *Phys. Rev. A* **81**, 012301 (2010).
- [29] D. L. McAuslan, P. M. Ledingham, W. R. Naylor, S. E. Beavan, M. P. Hedges, M. J. Sellars, and J. J. Longdell, Photon-echo quantum memories in inhomogeneously broadened two-level atoms, *Phys. Rev. A* **84**, 022309 (2011).
- [30] A. Arcangeli, A. Ferrier, and P. Goldner, Stark echo modulation for quantum memories, *Phys. Rev. A* **93**, 062303 (2016).
- [31] A. L. Alexander, J. J. Longdell, M. J. Sellars, and N. B. Manson, Photon Echoes Produced by Switching Electric Fields, *Phys. Rev. Lett.* **96**, 043602 (2006).
- [32] M. P. Hedges, J. J. Longdell, Y. Li, and M. J. Sellars, Efficient quantum memory for light, *Nature (London)* **465**, 1052 (2010).
- [33] T. Chanelière and G. Hétet, Light-shift-modulated photon-echo, *Opt. Lett.* **40**, 1294 (2015).
- [34] B. S. Ham, A controlled ac Stark echo for quantum memories, *Sci. Rep.* **7**, 7655 (2017).
- [35] T. Zhong, J. M. Kindem, J. G. Bartholomew, J. Rochman, I. Craiciu, E. Miyazono, M. Bettinelli, E. Cavalli, V. Verma, S. W. Nam, F. Marsili, M. D. Shaw, A. D. Beyer, and A. Faraon, Nanophotonic rare-earth quantum memory with optically controlled retrieval, *Science* **357**, 1392 (2017).
- [36] S. P. Horvath, M. K. Alqedra, A. Kinos, A. Walther, J. M. Dahlström, S. Kröll, and L. Rippe, Noise free on-demand atomic-frequency comb quantum memory, *arXiv:2006.00943*.
- [37] I. Craiciu, M. Lei, J. Rochman, J. G. Bartholomew, and A. Faraon, Multifunctional on-chip storage at telecommunication wavelength for quantum networks, *Optica* **8**, 114 (2021).
- [38] M. Hosseini, B. M. Sparkes, G. Hétet, J. J. Longdell, P. K. Lam, and B. C. Buchler, Coherent optical pulse sequencer for quantum applications, *Nature (London)* **461**, 241 (2009).
- [39] K. I. Gerasimov, S. A. Moiseev, and R. B. Zaripov, Microwave spin frequency comb memory protocol controlled by gradient magnetic pulses, *Appl. Magn. Reson.* **48**, 795 (2017).
- [40] V. Giovannetti, S. Lloyd, and L. Maccone, Quantum Random Access Memory, *Phys. Rev. Lett.* **100**, 160501 (2008).
- [41] E. S. Moiseev and S. A. Moiseev, Time-bin quantum RAM, *J. Mod. Opt.* **63**, 2081 (2016).
- [42] C. Simon, H. de Riedmatten, M. Afzelius, N. Sangouard, H. Zbinden, and N. Gisin, Quantum Repeaters with Photon Pair Sources and Multimode Memories, *Phys. Rev. Lett.* **98**, 190503 (2007).
- [43] S. A. Moiseev, S. N. Andrianov, and F. F. Gubaidullin, Efficient multimode quantum memory based on photon echo in an optimal QED cavity, *Phys. Rev. A* **82**, 022311 (2010).
- [44] M. Afzelius and C. Simon, Impedance-matched cavity quantum memory, *Phys. Rev. A* **82**, 022310 (2010).
- [45] N. S. Perminov, D. Y. Tarankova, and S. A. Moiseev, Super-efficient cascade multiresonator quantum memory, *Laser Phys. Lett.* **15**, 125203 (2018).
- [46] M. Sabooni, Q. Li, S. Kröll, and L. Rippe, Efficient Quantum Memory using a Weakly Absorbing Sample, *Phys. Rev. Lett.* **110**, 133604 (2013).
- [47] P. Jobez, I. Usmani, N. Timoney, C. Laplane, N. Gisin, and M. Afzelius, Cavity-enhanced storage in an optical spin-wave memory, *New J. Phys.* **16**, 083005 (2014).
- [48] R. A. Akhmedzhanov, L. A. Gushchin, A. A. Kalachev, N. A. Nizov, V. A. Nizov, D. A. Sobgayda, and I. V. Zelensky, Cavity-assisted atomic frequency comb memory in an isotopically pure <sup>143</sup>Nd<sup>3+</sup>: YLiF<sub>4</sub> crystal, *Laser Phys. Lett.* **13**, 115203 (2016).
- [49] W. B. Mims, Phase memory in electron spin echoes, lattice relaxation effects in CaWO<sub>4</sub>: Er, Ce, Mn, *Phys. Rev.* **168**, 370 (1968).

- [50] See Supplemental Material at <http://link.aps.org/supplemental/10.1103/PhysRevB.103.174110> for the details about the analysis of electrical field inhomogeneities in the electrode circuit, impedance-matched cavity parameters, and the derivation of equation for the ROSE echo efficiency.
- [51] Y. Sun, G. M. Wang, R. L. Cone, R. W. Equall, and M. J. M. Leask, Symmetry considerations regarding light propagation and light polarization for coherent interactions with ions in crystals, *Phys. Rev. B* **62**, 15443 (2000).
- [52] M. S. Silver, R. I. Joseph, and D. I. Hoult, Selective spin inversion in nuclear magnetic resonance and coherent optics through an exact solution of the Bloch-Riccati equation, *Phys. Rev. A* **31**, 2753 (1985).
- [53] I. Roos and K. Mølmer, Quantum computing with an inhomogeneously broadened ensemble of ions: Suppression of errors from detuning variations by specially adapted pulses and coherent population trapping, *Phys. Rev. A* **69**, 022321 (2004).
- [54] A. Abragam, *The Principles of Nuclear Magnetism*, International Series of Monographs on Physics (Clarendon Press, Oxford, 1989).
- [55] M. M. T. Loy, Observation of Population Inversion by Optical Adiabatic Rapid Passage, *Phys. Rev. Lett.* **32**, 814 (1974).
- [56] F. T. Hioe, Solution of Bloch equations involving amplitude and frequency modulations, *Phys. Rev. A* **30**, 2100 (1984).
- [57] R. M. Macfarlane, Optical Stark spectroscopy of solids, *J. Lumin.* **125**, 156 (2007).
- [58] A. J. Meixner, C. M. Jefferson, and R. M. Macfarlane, Measurement of the Stark effect with subhomogeneous linewidth resolution in  $\text{Eu}^{3+} : \text{YAlO}_3$  with the use of photon-echo modulation, *Phys. Rev. B* **46**, 5912 (1992).
- [59] J. G. Bartholomew, T. Zhong, J. M. Kindem, R. Lopez-Rios, J. Rochman, I. Craiciu, E. Miyazono, and A. Faraon, Controlling rare-earth ions in a nanophotonic resonator using the ac Stark shift, *Phys. Rev. A* **97**, 063854 (2018).
- [60] B. Z. Malkin, D. S. Pytalev, M. N. Popova, E. I. Baibekov, M. L. Falin, K. I. Gerasimov, and N. M. Khaidukov, Random lattice deformations in rare-earth-doped cubic hexafluoroelpasolites: High-resolution optical spectroscopy and theoretical studies, *Phys. Rev. B* **86**, 134110 (2012).
- [61] N. M. Abishev, E. I. Baibekov, B. Z. Malkin, M. N. Popova, D. S. Pytalev, and S. A. Klimin, Deformation broadening and the fine structure of spectral lines in optical spectra of dielectric crystals containing rare-earth ions, *Phys. Solid State* **61**, 795 (2019).
- [62] N. M. Arslanov and S. A. Moiseev, Multimode photon echo quantum memory in the medium with longitudinal inhomogeneous broadening, *Uch. Zap. Kaz. Univ. Ser. Fiz.-Mat. Nauk.* **152**, 27 (2010).
- [63] M. P. Hedges, High performance solid state quantum memory, Ph.D. thesis, Australian National University, 2011, <http://hdl.handle.net/1885/150814>.
- [64] G. Armagan, A. M. Buoncristiani, and B. Di Bartolo, Excited state dynamics of thulium ions in Yttrium Aluminum Garnets, *Opt. Mater. (Amsterdam)* **1**, 11 (1992).
- [65] S. A. Moiseev, Some general nonlinear properties of photon-echo radiation in optically dense media, *Opt. Spectrosc.* (English translation of *Optika i Spektroskopiya*) **62**, 180 (1987).
- [66] R. Urmancheev, K. Gerasimov, M. Minnegaliev, T. Chanelière, A. Louchet-Chauvet, and S. Moiseev, Two-pulse photon echo area theorem in an optically dense medium, *Opt. Express* **27**, 28983 (2019).
- [67] S. A. Moiseev, M. Sabooni, and R. V. Urmancheev, Photon echoes in optically dense media, *Phys. Rev. Research* **2**, 012026(R) (2020).
- [68] F. Könz, Y. Sun, C. W. Thiel, R. L. Cone, R. W. Equall, R. L. Hutcheson, and R. M. Macfarlane, Temperature and concentration dependence of optical dephasing, spectral-hole lifetime, and anisotropic absorption in  $\text{Eu}^{3+} : \text{Y}_2\text{SiO}_5$ , *Phys. Rev. B* **68**, 085109 (2003).
- [69] T. Böttger, C. W. Thiel, R. L. Cone, and Y. Sun, Effects of magnetic field orientation on optical decoherence in  $\text{Er}^{3+} : \text{Y}_2\text{SiO}_5$ , *Phys. Rev. B* **79**, 115104 (2009).